# "On-the-fly" synthesis of self-supported LDH hollow structures through controlled microfluidic reaction-diffusion conditions

Michele Mattera,[a] Alessandro Sorrenti,[b] Lidia De Gregorio Perpiñá,[a] Víctor Oestreicher,[c] Semih Sevim,[d] Xiang-Zhong Chen,[e] Salvador Pané,[d] Gonzalo Abellán*[c] and Josep Puigmartí-Luis*[a,f]

a Departament de Ciència dels Materials i Química Física, Institut de Química Teòrica i Computacional, University of Barcelona (UB), 08028 Barcelona, Spain

b Departament de Química Inorgànica i Orgànica (Secció de Química Orgànica), University of Barcelona (UB), 08028 Barcelona, Spain

c Institute of Molecular Science, University of Valencia (UVEG), c/ Catedrático José Beltrán 2, 46980 Paterna, Spain

d Institute of Robotics and Intelligent Systems, ETH Zurich, Tannenstrasse 3, Zurich CH 8092, Switzerland

e Institute of Optoelectronics, State Key Laboratory of Photovoltaic Science and Technology, Shanghai Frontiers Science Research Base of Intelligent Optoelectronics and Perception, Fudan University, Shanghai 200438, People's Republic of China.

f Institució Catalana de Recerca i Estudis Avançats (ICREA), Pg. Lluís Companys 23, 08010 Barcelona, Spain

**Abstract**

Layered double hydroxides (LDHs) are a class of functional materials that exhibit exceptional properties for diverse applications in areas such as heterogeneous catalysis, energy storage and conversion, and bio-medical applications, among others. Efforts have been devoted to produce millimeter-scale LDH structures for direct integration into functional devices. However, the controlled synthesis of self-supported continuous LDH materials with hierarchical structuring up to the millimeter scale through a straightforward one-pot reaction method remains unaddressed. Herein, we show that millimeter-scale self-supported LDH structures can be produced by means of a continuous flow microfluidic device in a rapid and reproducible one-pot process. Additionally, our microfluidic approach not only allows for an 'on-the-fly' formation of unprecedented LDH composite structures, but also for the seamless integration of millimeter-scale LDH structures into functional devices. Our method holds the potential to unlock the integrability of these materials, maintaining their performance and functionality, while diverging from conventional techniques like pelletization and densification that often compromise these aspects. Our strategy will enable exciting advancements in LDH performance and functionality.

## Introduction

Layered double hydroxides (LDHs), also referred to as anionic clays, are a sort of lamellar materials exhibiting a highly tuneable chemical composition.[1] Their chemical structure consists of infinite two-dimensional sheets comprising octahedral divalent (M(II)) and trivalent cations (M(III)) connected through $OH^-$ bridges.[2,3] These positively charged layers assemble through the inclusion of an (in)organic anion within their interlayer spaces. This arrangement gives rise to a plethora of inorganic as well as inorganic-organic hybrid materials with great potential in diverse application areas such as heterogeneous catalysis, energy storage and conversion, and biomedical applications, among others.[4–7]

Over the last decades, significant efforts have been dedicated to unravelling the structure-property relationship of LDHs.[8] Researchers have focused on investigating various factors that influence the properties of LDHs, including the M(II)/M(III) molar ratio,[9] the nature of the interlayer anion,[10] and/or the pH conditions employed during synthesis.[11] By carefully adjusting synthetic parameters, researchers have successfully demonstrated the ability to control the interlayer spacing, the charge density, and hence, the reactivity of LDHs.[12] Indeed, this trial-and-error optimization procedure has also enabled the customization of LDHs with specific functionalities, including enhanced catalytic activity,[13] controlled drug delivery,[14] and tailored adsorption and release properties.[15]

Research efforts have been also dedicated to exerting precise control over the nucleation, growth, crystal size and shape of LDHs.[5] This next level of control, spanning from the nanometer to the millimeter scale, is recognized as a critical parameter to enable the direct integration of these materials into ready-to-use functional devices. Significant advancements have been made in structuring LDHs, encompassing the fabrication of micrometric powders of porous nanoparticles,[16] as well as micro-structured millimeter-scale monoliths.[17] However, these achievements have been accomplished through multi-step and complex protocols including sol-gel techniques assisted by soft-templating methods,[18] and/or supported synthesis on diverse 2D or 3D solid supports, either through in-situ coprecipitation or self-assembly of preformed LDH

nanoparticles at the surface.[19] Despite the significant efforts towards the realization of millimeter-scale LDH structures, the preparation of self-supported LDH materials with controlled hierarchical structuring up to the millimeter scale using a straightforward one-pot reaction method remains unadressed.

Microfluidic technologies are emerging as a powerful toolkit in the field of materials science, offering precise control over the growth mechanisms of functional materials, i.e., over crystallization processes and self-assembly pathways.[20] Additionally, these technologies enable efficient processing and shaping of materials into various morphologies, providing new avenues for materials design and development. In particular, planar (i.e. 2D) continuous flow microfluidic devices operating under laminar flow conditions have proved to provide an exquisite spatiotemporal control over reaction-diffusion (RD) processes and reactant concentration gradients (with constant mass transfer of reactants to the RD area), as the mixing between the chemical species dissolved in co-flowing streams occurs solely through molecular diffusion. Note that in a planar continuous flow microfluidic device this diffusion process takes place at the vertical liquid-liquid interface formed within the microfluidic channel, where the two co-flowing reagent-laden fluid streams interact.[21] This configuration of the RD area allows for the creation of a distinct synthetic environment that is dramatically different from those encountered in conventional bulk synthetic methods, where chaotic turbulent mixing is employed to achieve a fast and perfect homogenization of the reactants, at the expense of losing control over the RD phenomena.[20] For example, our previous research has shown that the utilization of the advanced spatiotemporal mixing achieved with a planar continuous flow microfluidic device enables control over the internal structure of a conductive supramolecular polymer. This level of control is typically unattainable using conventional synthetic approaches, which rely on turbulent mixing conditions, unless different molecular building blocks are employed.[22] Additionally, the RD conditions achieved at the vertical liquid-liquid interface, generated within the main channel height in planar continuous flow microfluidic devices, have also facilitated the precise control over morphogenesis during the microfluidic synthesis of a coordination polymer, allowing for the

isolation of non-equilibrium intermediates.[23] The utilization of the same planar microfluidic device played also a crucial role in determining the degree of defects within the crystal structure of a spin-crossover material, thus also influencing its spin transition behavior.[24] Additionally, served as a pivotal tool in unveiling unprecedented growth pathways during the synthesis of a metal-organic framework (MOF).[25] In addition to enabling the controlled synthesis of different functional materials, the planar continuous flow microfluidic devices used in the aforementioned studies have also allowed for the direct printing of those materials, which otherwise are challenging to process using conventional bulk solvothermal methods, such as covalent organic frameworks (COFs).[26]

Herein, we demonstrate, for the first time, the utilization of a continuous flow microfluidic device for the controlled synthesis of millimeter-scale self-supported LDH hollow structures in a rapid (ca. 2 seconds) and reproducible one-pot reaction process. We introduce a different fluid stream configuration where the liquid-liquid interface has been transformed from a vertical arrangement to a concentric one employing a 3D hydrodynamic flow focusing set-up. This re-shaping of the liquid-liquid interface enables the expansion of the RD area beyond the limited height of the microfluidic channel typically found in planar continuous flow microfluidic devices. As a result, our findings conclusively demonstrate that the utilization of this concentric liquid-liquid interface serves as an ideal synthetic template, enabling superior control over the assembly and templated growth of self-supported LDH tubes under RD conditions. Furthermore, we demonstrate that the adoption of this concentric fluid stream configuration also enables an 'on-the-fly' formation of LDH-based composite structures that can be directly integrated into a device for characterization and function analysis. Specifically, we demonstrate the successful generation of millimeter-scale LDH@carbon nanotubes (CNTs) hollow structures, exhibiting similar morphology and size to the bare LDH hollow structures produced with the same concentric liquid-liquid interface approach. The developed LDH@CNTs composite structures display electrical transport properties, highlighting the potential of our methodology as a viable solution for the direct integration of LDHs and LDH-based composites into various devices. Note that the successful

direct integration of millimetre scale LDH-based structures presents exciting opportunities for advancing performance and functionality in a range of applications, including sensing or energy storage and conversion.

**Results and Discussion**

The formation of LDH hollow structures relies on the precise control of the reactant mixing at the concentric liquid-liquid interface that we achieve by using a continuous 3D hydrodynamic flow focussing device, comprising a linear reaction channel (main channel) and three inlet ports (Figure 1A). The main channel consists of a microfluidic tubing with a cross-section (inner) diameter of 1 mm and length of 10 cm, opportunely hold in place by a 3D printed plastic holder (see the supporting information (SI) for further details). Note that the solution injected through the central inlet (Flow 2 in Figure 1A) remains surrounded and focussed in the centre of the main channel by a concentric sheath created by the solutions injected through the lateral inlets (Flow 1 in Figure 1A). When operating this microfluidic device, two important parameters must be taken into account: i) the total flow rate (TFR), i.e., the sum of the flow rates of the solutions injected into the three inlets, which determines the total residence time of the reactants in the device; and ii) the flow rate ratio (FRR), defined as the ratio of the sheath flows to the central inlet flow, which determines the diameter of the concentric RD area generated between the sheath and central inlet flows, shown in pink in Figure 1B. To characterize the hydrodynamic properties of our microfluidic device, while directly visualizing the effect of the FRR on the hydrodynamic flow focussing, we performed preliminary experiments using a blue food dye (Figure S1). In these experiments, the dye was introduced through the central inlet (i.e. Flow 2 inlet), while water was simultaneously injected through the two lateral inlets (i.e. the two Flow 1 inlets). This deliberate configuration led to the creation of a concentric liquid-liquid interface, effectively confining the blue dye-laden stream to the middle section of the main channel (Figure S1). When the FRR was increased from 2 to 20, the hydrodynamic flow focussing clearly increased with an evident squeezing of the blue dye-laden stream. For example, we observed that at a distance of 1 mm from the microfluidic tubing's tip downstream of the primary channel, the cross-sectional area of

the blue dye-laden stream decreased from approximately 331,830 µm² at a FRR of 2 to roughly 25,446 µm² when the FRR was increased to 20. Notably, throughout this range of FRRs, the flow profile remained stable without any observed turbulence.

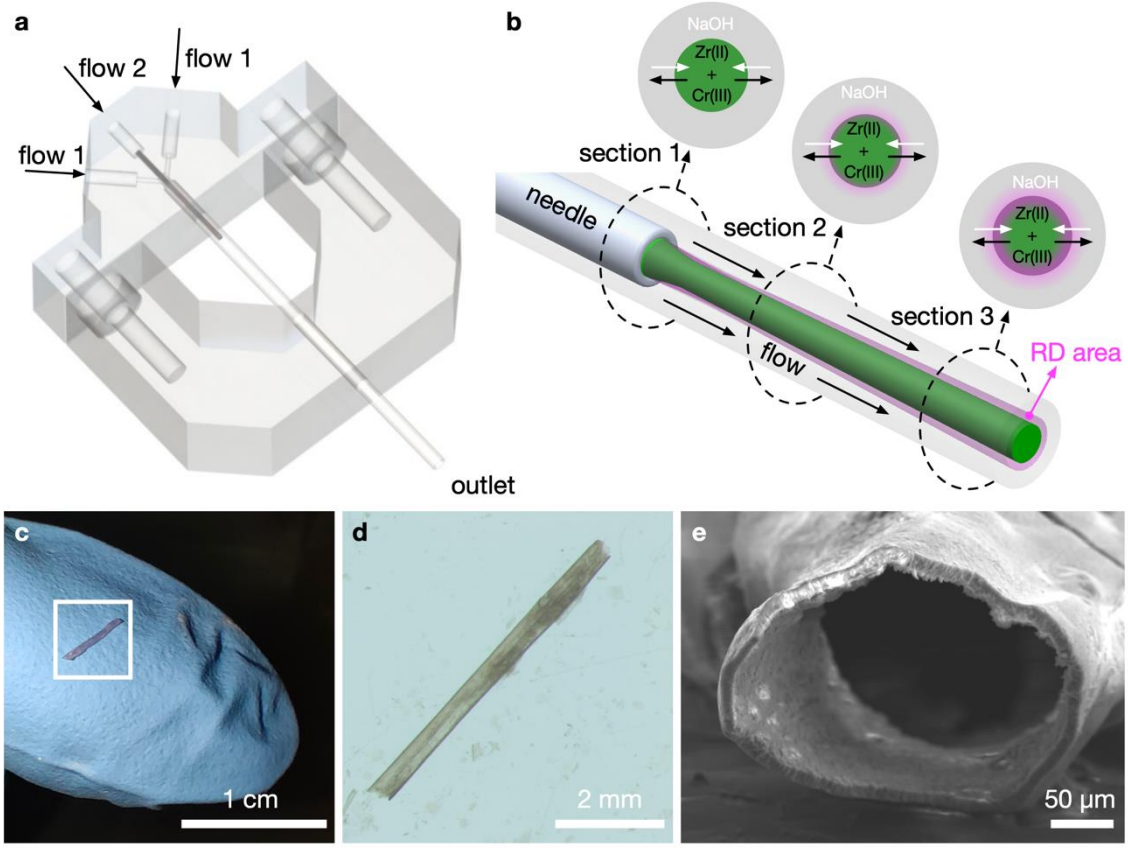


**Figure 1**. Schematic illustrations showing both, the continuous flow microfluidic device (a), and the progressive development of the RD area, which occurs downstream along the main channel (b). Note that the RD area (shown in pink in Figure 1B) is strategically positioned at the concentric liquid-liquid interface. (c) and (d) micrographs of millimetric ZnCr LDH hollow fibres. (e) SEM image of a ZnCr LDH hollow fibre showing its micrometric wall thickness along with the distinctive hollow interior.

To investigate the formation of LDHs using this continuous flow microfluidic device, we selected ZnCr LDH as our model system. This selection is based on the high stability of ZnCr LDH, and the growth behavior of Cr-based LDHs, which undergoes a single precipitation step at pH values

higher than 5, making it a well suitable model system for synthesis control through modulation of microfluidic parameters (*vide infra*).

In a typical experiment, we injected an acidic solution (pH = 3) containing the two metal cations, $Zn^{2+}$ and $Cr^{3+}$, with a Zn/Cr ratio of 2:1, through the central inlet of the microfluidic device (i.e. through Flow 2). Simultaneously, an alkaline solution of NaOH (2 M) was injected through the lateral inlets (i.e. through Flow 1), serving as the precipitating agent for the reaction. Note that this experimental setup enables to establish the concentric liquid-liquid interface between the central laden stream transporting the metal cations and the alkaline sheath surrounding it. In addition, diffusion of the metal ions outward of the middle stream, and of NaOH towards the centre of the main channel, creates well-defined concentration and pH gradients at each channel cross-section while the injected solutions move downstream the main channel (i.e. steady state gradients are being generated, see Figure 1B). Since under laminar flow conditions the mixing of reactants is solely mediated by a diffusion-limited process, the ZnCr LDH growth is confined to specific regions surrounding the concentric liquid-liquid interface where the cation concentration and pH reach optimal values for nucleation and subsequent growth of the ZnCr LDH material. In addition, the continuous injection of the solutions inside this microfluidic device ensures a continuous supply of precursors at the nucleation and growth region. This continuous supply prevents a depletion regime and enables a continuous synthesis. As a result, millimetre long self-supported hollow tubular structures are formed in approximately 2 seconds (i.e., the residence time), and are collected directly at the outlet of the microfluidic device (Figure 1C, 1D and 2A).

In order to find the best operating conditions for the synthesis of the self-supported hollow tubular structures, we screened the microfluidic parameters TFR (within the range 1050-4200 µL/min) and FRR (from 0.3 to 10), and we could identify combinations of values of these parameters which enable the formation of self-supported hollow structures (see Table S1 in SI). For example, when the microfluidic synthesis was performed at TFR 2100 µL/min and FRR of 3 (see SI for further details), we could achieve the continuous formation of insoluble straight self-supported hollow structures, with a purple colour and length of several millimetres, which could be easily

washed and isolated, as shown in Figure 1C. Although the presence of an internal cavity was quite recognizable by optical microscopy (Figure 1D), it was unambiguously confirmed by scanning electron microscopy (SEM) as shown in Figure 1E. During the preparation of SEM samples, which involved depositing the hollow structures onto carbon tape followed by gold sputtering, we cracked opened some hollow structures to measure the wall thickness which were found to be in the order of tens of microns (see Table S1 and Figure S2 and S3). The small wall thickness clearly suggests that the reaction/precipitation occurs in a very narrow and localized zone within the concentric liquid-liquid interface. Interestingly, the external surface of self-supported hollow structures (grown in contact with the alkaline solution) appears to be smoother than the inner surface (Figure S2). The elemental composition analysis, performed using energy dispersive X-ray spectroscopy (EDS) confirmed the presence of both metals ($Zn^{2+}$ and $Cr^{3+}$) in the expected 2:1 theoretical ratio, as well as of oxygen, as shown in Figure S4 and Table S2.

Note that this control over the size and shape of self-supported hollow structures cannot be achieved with conventional synthetic approaches. For the sake of comparison, we also did the reaction using a conventional co-precipitation method. This involved a bulk mixing of the acidic solution containing the metal cations with a NaOH solution. Namely, we used the same precursor solutions as the ones injected in the microfluidic device. To facilitate a rapid and turbulent mixing of the reagents, we employed vigorous vortex stirring. Subsequently, the reaction mixture was left at room temperature for a duration of 2 hours, leading to the precipitation of a purple powder (Figure 2D) containing both metals in the expected 2:1 ratio, as confirmed by EDS (Figure S5 and Table S2). Moreover, SEM images of the obtained product showed a heterogeneous morphology of the solid powder, demonstrating that the conventional synthetic approach did not provide any control over the size or shape of the obtained material, as shown in Figure S6.

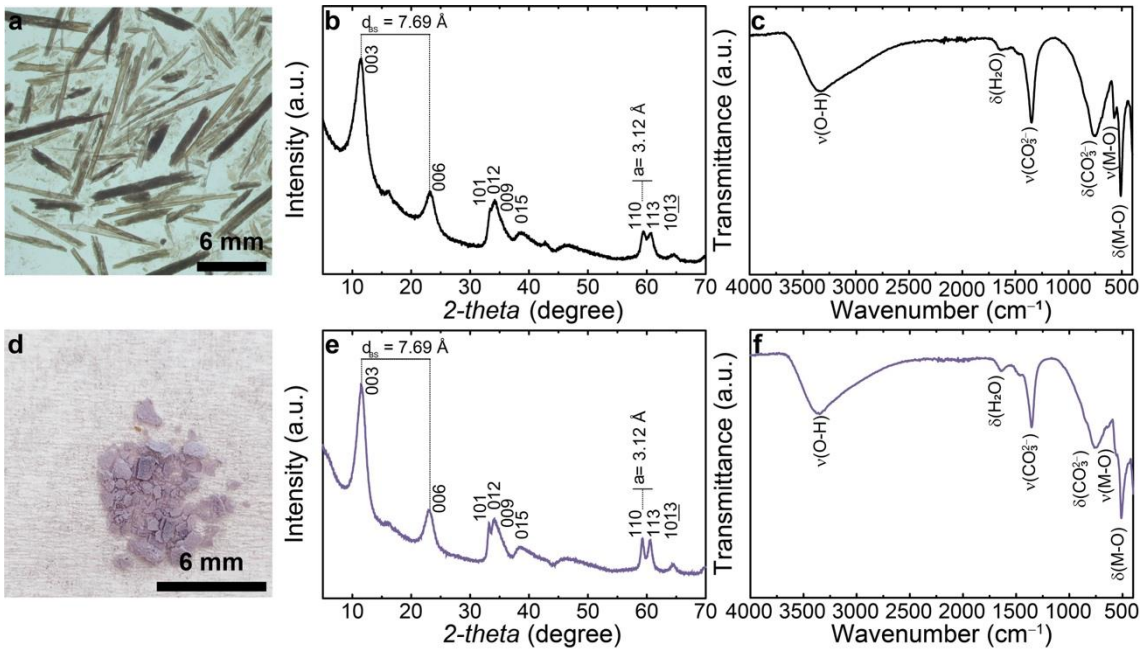


**Figure 2.** (a) Optical microscope image of ZnCr LDH hollow structures. (b) PXRD pattern and (c) FTIR–ATR spectrum of ZnCr LDH hollow structures. (d) Micrograph of the ZnCr LDH powder produced in bulk under turbulent mixing. (e) PXRD pattern and (f) FTIR–ATR spectrum of the ZnCr LDH powder.

To unequivocally confirm the ZnCr LDH nature of both the self-supported hollow structures and the bulk powder, we performed powder X-ray diffraction (PXRD) measurements. The corresponding PXRD diffraction patterns are shown in Figure 2B and 2E, respectively, revealing coincident reflections at 11.5, 23.0, 34.0, 38.5, 42.8, 59.4, 60.6 and 64.8º. These patterns exhibit excellent agreement with the diffraction pattern previously reported for the *hydrotalcite*-like structure of ZnCr LDH, confirming the formation of the desired crystalline material.[27] Specifically, the basal space distance ($d_{BS}$) and intralayer parameter ($a$) are in perfect agreement with the ZnCr LDH phase.[28] Further, the Fourier transform infrared spectra attenuated total reflectance (FTIR–ATR) of both the self-supported hollow structures and bulk material (Figure 2C and 2F respectively) display vibrations at 3280 $cm^{-1}$, corresponding to the -OH stretching, at 650 and 500 $cm^{-1}$, associated with the M-O bonds, as well as bands at 1350 and 750 $cm^{-1}$, indicating the presence of carbonate ($CO_3^{2-}$) as the intercalating anion.[29] In fact, the use of a

strongly alkaline solution for the synthesis of the ZnCr LDH (both in microfluidic and bulk conditions) favours the capture and solubilization of atmospheric carbon dioxide, which is thus present as intercalant in the LDH structure (as carbonate ion $CO_3^{2-}$). Carbonate has a strong interaction with the hydroxide layer and quickly exchanges the counter anion from the precursors metal salts, namely $Cl^-$, in the LDH structure, as also in agreement with the basal space distance ($d_{BS}$) of 7.69Å observed in the PXRD patterns.

To further showcase the versatility of our microfluidic approach, we decided to decrease the TFR during the fabrication of the self-supported ZnCr LDH hollow structures from 2100 µL/min to 1050 µL/min while keeping the FRR at 3. This deliberate modification was aimed at facilitating the enhanced diffusion of the two metal cations and alkaline solution along the main channel and towards the outlet. We sought to increase the diffusion of reactants inside the RD area (i.e. the reaction area) to facilitate the formation of non-hollow ZnCr LDH fibres. Remarkably, our observations revealed a consistent trend wherein exclusively non-hollow fibers were generated across the entire spectrum of conditions, ranging from a FRR of 2 to 10, while maintaining the TFR at 1050 µL/min (Table S1 and Figure S7). As shown in Figure S8, the obtained PXRD data unequivocally confirmed that all the non-hollow fibers produced at a TFR of 1050 µL/min and FRR of 2, 3, or 10 are indeed composed of ZnCr LDH. Furthermore, when we increased the TFR beyond 2100 µL/min (e.g. to 4200 µL/min), we observed the formation of non-complete hollow structures. These results clearly indicate that at TFRs exceeding 2100 µL/min (i.e., for shorter residence times), the time available for the diffusion of reactants inside the concentric RD area is insufficient to achieve the closure (or complete assembly) of the hollow structures (Figure S9). PXRD analysis confirmed that also these non-complete hollow structures are composed of ZnCr LDH (Figures S8).

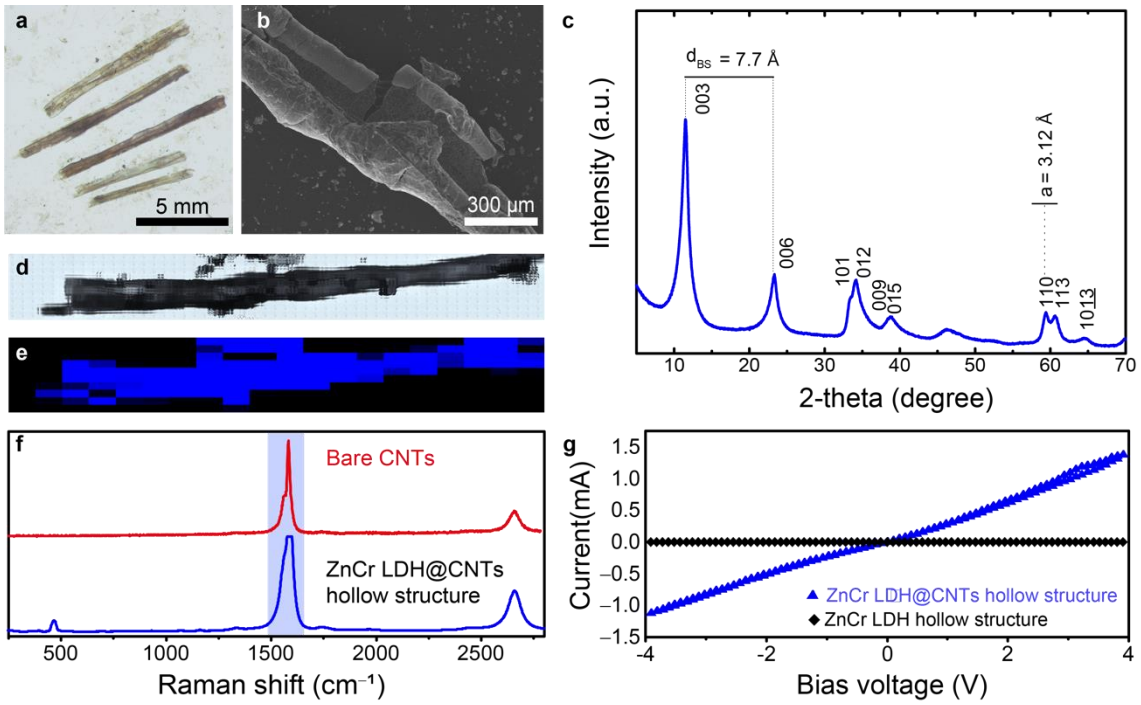


**Figure 3.** (a) Optical microscope and (b) SEM images of ZnCr LDH@CNTs hollow structures. (c) PXRD pattern of the ZnCr LDH@CNTs hollow structures. (d) and (e) Optical microscope and Raman map of a ZnCr LDH@CNTs hollow structure. The Raman map presented in (e) is acquired at 1580 $cm^{-1}$ (i.e., at the G band of CNTs) highlighted in blue in Figure 3f. (f) Raman spectra of CNTs (red) and ZnCr LDH@CNTs hollow structures (black). (g) I/V sweeps of a ZnCr LDH hollow structure (blue) and a ZnCr LDH@CNTs hollow structure (black).

From an application perspective, LDHs are emerging as promising materials for a variety of electrochemical applications, including sensing, energy storage and conversion.[30,31] Nevertheless, one main drawback in this field lies in the inherent insulating behaviour of bare LDHs, which can be overcome by the generation of hybrid-materials in which LDHs are blended with a conductive carbon matrix.[32] Capitalizing on the capability to fabricate millimeter scale self-supported ZnCr LDHs hollow structures through our dynamic and concentric microfluidic-based liquid-liquid interface, we explored the possibility of preparing a self-supported ZnCr LDH@carbon nanotubes (CNTs) composite material utilizing the same one-pot microfluidic-based reaction process. Note that the synthesis of self-supported LDH-based materials with controlled hierarchical structuring

at the millimeter scale using a simple one-pot reaction method has remained largely unexplored in the scientific community, however, there is a pressing need for the development of such technology to significantly enhance the performance, functionality, and seamless integration of LDH-based materials into ready-to-use devices.

To address this grand challenge, we made modifications to the microfluidic synthesis protocol used during the formation of self-supported ZnCr LDH hollow structures by introducing a dispersion of commercial CNTs (i.e. TUBALL-BATT-H2O) in addition to the NaOH solution through the lateral inlets (i.e., the two Flow 1 in Figure 1A). Similar to the previous synthesis, the two metal cations, $Zn^{2+}$ and $Cr^{3+}$ (with a Zn/Cr ratio of 2:1) were injected through the central inlet of the microfluidic device (see SI for further details for this synthetic procedure). Note that the CNT source used in our work has been commonly employed to create hybrid conductive composites with enhanced water solubility and stability, features that are achieved by using carboxymethyl cellulose as modifier agent in its formulation. Interestingly, we observed that the presence of suspended CNTs did not significantly affect the hydrodynamic stability of our reagent-laden flows. As a result, we could still achieve a continuous formation of hollow structures with lengths of several millimetres in approximately 2 seconds, but in this case showing a darker colour, along with black striations, suggesting the incorporation of the carbon-based material (Figure 3A). Indeed, PXRD measurements confirmed the formation of the ZnCr LDH composite material, without noting any variation of the basal distance (Figure 3C), suggesting a localisation of the CNTs outside the LDH crystalline domains. Additionally, the SEM images also verified the hollow structure of the self-supported ZnCr LDH@CNTs composite material, with a wall thickness comparable to that of the bare ZnCr LDH hollow structures (Figure 3B). The SEM analysis revealed that the CNTs were predominantly absorbed onto the external smooth surface of the ZnCr LDH@CNTs hollow structures, creating a distinctive network-like layer (Figure S10). To demonstrate the presence of CNTs in the ZnCr LDH@CNTs hollow structures, we employed confocal Raman microscopy. As shown in Figure 3F, the Raman spectra obtained clearly confirmed the presence of CNTs from the appearance of their characteristic bands located

at ca. 1580 $cm^{-1}$ (intense G band originated from the in-plane lattice vibrations) and at ca. 2650 $cm^{-1}$ (second overtone of the G band). These Raman vibrations correspond to those measured for the CNTs coming from the precursor CNT solution. Conversely, bare ZnCr LDH hollow fibres do not show any Raman signal in this region of the spectra (data not shown). The Raman mapping of a single isolated ZnCr LDH@CNTs hollow structure at the intensity of the G band (i.e. at 1580 $cm^{-1}$) clearly demonstrated that the CNTs are uniformly spread all over the external area of the composite hollow structure (Figure 3D and Figure 3E). Taken all together, these observations unequivocally confirm the successful formation of millimetre-long ZnCr LDH@CNTs hollow structures with our synthetic one-pot microfluidic approach and only requiring around 2 seconds. Next, and taking advantage of the direct integration that can be accomplished with these millimetre-long ZnCr LDH@CNTs hollow structures, we prepared a two-point resistance-measuring device at the level of the single composite hollow structure to study its conductivity properties (Figures S11-13). As an internal reference, we used a bare ZnCr LDH hollow structure mounted nearby a ZnCr LDH@CNT hollow structure (Figure S12-13). Upon applying a voltage across the two electrodes connected to the ZnCr LDH@CNTs hollow structure, we observed a distinct ohmic behavior in the acquired I/V sweeps, as reported in Figure 3G. Conversely, the bare ZnCr LDH hollow structure exhibited the anticipated insulating properties (Figure 3G). Based on these measurements, we were able to make a qualitative estimation of the equivalent resistance of the ZnCr LDH@CNTs hollow fiber, which falls in the kilo-ohm range (ca. 2,5 kΩ). In comparison to other LDH@carbon-based composite materials, this magnitude of resistance is high. Typically, LDH@carbon composites exhibit significantly lower resistance values, often ranging in milli-ohms or even micro-ohms.[33] However, it is important to note that these conductivity measurements for reported LDH@carbon-based composites are usually conducted after pelletization and densification methods, exclusively assessing the pressed composite materials devoid of any hierarchical control. Notably, in this study, we achieved a groundbreaking feat by successfully measuring a single self-supported ZnCr LDH@CNTs hollow structure without any post-processing (i.e., pelletization and densification) and after its direct integration into the measuring device. Moreover, the ZnCr LDH@CNTs hollow structure demonstrates

robustness, as multiple measurements were conducted at high voltage values, such as up to 4V, without any change observed in the I/V sweep measurements. This highlights the excellent durability and stability of the self-supported hollow composite structures fabricated with our home-made microfluidic approach.

## Conclusions

In summary, our study demonstrates that redesigning the liquid-liquid interface in a continuous flow microfluidic device, transitioning from a vertical to a circular configuration, not only enables the generation of self-supported ZnCr LDH hollow structures in around 2 seconds but it also facilitates the one-pot synthesis of conductive composites like the ZnCr LDH@CNTs hollow structures presented in this work. These results unequivocally demonstrate that the proposed technology is exceptionally well-suited for creating unprecedented self-supported hierarchical structures that can be directly integrated into functioning devices without the need for pelletization and/or densification approaches. Importantly, our method also eliminates the need for well-established multi-step and complex protocols like soft-templating methods or supported synthesis on 2D or 3D solid supports to achieve free-standing LDH structures at the millimeter scale. Furthermore, to highlight the versatility of our approach in generating self-supporting structures without relying on well-established multi-step and complex protocols, we have also synthesized unprecedented NiCo layered hydroxides (LH) hollow structures in their α phase in approximately 2 seconds (see Figures S14-15). Note that α-NiCo LH is only generated under solvothermal conditions, and obtained in a powder form, after several hours of reaction.[34,35] Therefore, the ability to generate these self-supported inorganic-based or composite structures at room temperature and in a significantly shorter time scale (i.e., seconds) opens up a new era of possibilities in materials engineering. We believe that our findings will inspire further research and innovation in the field of inorganic-based or composite LDH structures, pushing the boundaries of what can be achieved through continuous flow microfluidic devices and driving the scientific community towards exciting new frontiers in advanced materials design as well as in the fabrication of functional devices with targeted performances.

**Acknowledgment**

This work is supported by the Swiss National Science Foun-dation (project no. 200021_181988, IZLCZ0_206033) and grant PID2020-116612RB-C33 funded by MCIN/ AEI /10.13039/501100011033. S.P. and J.P-L. also acknowledge support from the European Union's Horizon Europe Research and Innovation Programme under the EVA project (GA No: 101047081). J.P-L. acknowledges the Agencia Estatal de Investigación (AEI) for the María de Maeztu, project no. CEX2021-001202-M. Additionally, G.A. also acknowledges the European Research Council (ERC Starting Grant 2D PnictoChem No. 804110 and ERC Proof of Concept Grant 2D4H2 No. 101101079), the Spanish MICIN (Projects PID2019-111742GA-I00, Unit of Excellence "Maria de Maeztu" CEX2019-000919-M and TED2021-131347B-I00) and the Generalitat Valenciana (CIDEGENT/2018/001). V.O. also thanks ALN's membership.

**References**

(1) Vaccari, A. Layered Double Hydroxides: Present and FutureV. Rives (Ed.), Nova Science Publishers, Inc., New York, 2001, IX+439 Pp., ISBN 1-59033-060-9. *Appl. Clay Sci.* **2002**, *22* (1–2), 75–76.

(2) Wang, Q.; O'Hare, D. Recent Advances in the Synthesis and Application of Layered Double Hydroxide (LDH) Nanosheets. *Chem. Rev.* **2012**, *112* (7), 4124–4155.

(3) He, S.; An, Z.; Wei, M.; Evans, D. G.; Duan, X. Layered Double Hydroxide-Based Catalysts: Nanostructure Design and Catalytic Performance. *Chem. Commun.* **2013**, *49* (53), 5912.

(4) Mishra, G.; Dash, B.; Pandey, S. Layered Double Hydroxides: A Brief Review from Fundamentals to Application as Evolving Biomaterials. *Applied Clay Science*. Elsevier Ltd 2018, pp 172–186.

(5) Taviot-Guého, C.; Prévot, V.; Forano, C.; Renaudin, G.; Mousty, C.; Leroux, F.

Tailoring Hybrid Layered Double Hydroxides for the Development of Innovative Applications. *Adv. Funct. Mater.* **2018**, *28* (27), 1703868.

(6) Abellán, G.; Martí-Gastaldo, C.; Ribera, A.; Coronado, E. Hybrid Materials Based on Magnetic Layered Double Hydroxides: A Molecular Perspective. *Acc. Chem. Res.* **2015**, *48* (6), 1601–1611.

(7) Carrasco, J. A.; Oestreicher, V.; Silva, A. S.-D.; Abellán, G. Magnetism in Two-Dimensional Layered Double Hydroxides. *Appl. Clay Sci.* **2023**, *243*, 107073.

(8) He, S.; Han, J.; Shao, M.; Liang, R.; Wei, M.; Evans, D. G.; Duan, X. Layered Double Hydroxides: Structure-Property Relationships. In *Handbook of Solid State Chemistry*; Wiley-VCH Verlag GmbH & Co. KGaA: Weinheim, Germany, 2017; pp 541–569.

(9) Zhang, Z.; Chen, G. A Convenient Chemical Titration Method to Measure M( <scp>ii</Scp> )/M( <scp>iii</Scp> ) Ratios of Layered Double Hydroxides. *RSC Adv.* **2014**, *4* (59), 31333.

(10) Hibino, T. Anion Selectivity of Layered Double Hydroxides: Effects of Crystallinity and Charge Density. *Eur. J. Inorg. Chem.* **2018**, *2018* (6), 722–730.

(11) Kameliya, J.; Verma, A.; Dutta, P.; Arora, C.; Vyas, S.; Varma, R. S. Layered Double Hydroxide Materials: A Review on Their Preparation, Characterization, and Applications. *Inorganics* **2023**, *11* (3), 121.

(12) Rojas, R.; Giacomelli, C. E. Effect of Structure and Bonding on the Interfacial Properties and the Reactivity of Layered Double Hydroxides and Zn Hydroxide Salts. *Colloids Surfaces A Physicochem. Eng. Asp.* **2013**, *419*, 166–173.

(13) Xu, Z. P.; Zhang, J.; Adebajo, M. O.; Zhang, H.; Zhou, C. Catalytic Applications of Layered Double Hydroxides and Derivatives. *Appl. Clay Sci.* **2011**, *53* (2), 139–150.

(14) Kura, A. U.; Hussein, M. Z.; Fakurazi, S.; Arulselvan, P. Layered Double Hydroxide Nanocomposite for Drug Delivery Systems; Bio-Distribution, Toxicity and Drug

Activity Enhancement. *Chem. Cent. J.* **2014**, *8* (1), 47.

(15) Bullo, S.; Hussein, M. Z. Inorganic Nanolayers: Structure, Preparation, And Biomedical Applications. *Int. J. Nanomedicine* **2015**, 5609.

(16) Sun, Y.; Zhou, J.; Cai, W.; Zhao, R.; Yuan, J. Hierarchically Porous NiAl-LDH Nanoparticles as Highly Efficient Adsorbent for p-Nitrophenol from Water. *Appl. Surf. Sci.* **2015**, *349*, 897–903.

(17) Tokudome, Y.; Tarutani, N.; Nakanishi, K.; Takahashi, M. Layered Double Hydroxide (LDH)-Based Monolith with Interconnected Hierarchical Channels: Enhanced Sorption Affinity for Anionic Species. *J. Mater. Chem. A* **2013**, *1* (26), 7702.

(18) Tokudome, Y.; Prevot, V.; Tarutani, N. Processing Porous Architectures Based on LDH: Synthesis and Novel Applications. *Appl. Clay Sci.* **2023**, *243*, 107051.

(19) Sadeghi Rad, T.; Khataee, A.; Sadeghi Rad, S.; Arefi-Oskoui, S.; Gengec, E.; Kobya, M.; Yoon, Y. Zinc-Chromium Layered Double Hydroxides Anchored on Carbon Nanotube and Biochar for Ultrasound-Assisted Photocatalysis of Rifampicin. *Ultrason. Sonochem.* **2022**, *82*, 105875.

(20) Sevim, S.; Sorrenti, A.; Franco, C.; Furukawa, S.; Pané, S.; Demello, A. J.; Puigmartí-Luis, J. Self-Assembled Materials and Supramolecular Chemistry within Microfluidic Environments: From Common Thermodynamic States to Non-Equilibrium Structures. *Chem. Soc. Rev.* **2018**, *47* (11), 3788–3803.

(21) Puigmartí-Luis, J. Microfluidic Platforms: A Mainstream Technology for the Preparation of Crystals. *Chem. Soc. Rev.* **2014**, *43* (7), 2253–2271.

(22) Puigmartí-Luis, J.; Schaffhauser, D.; Burg, B. R.; Dittrich, P. S. A Microfluidic Approach for the Formation of Conductive Nanowires and Hollow Hybrid Structures. *Adv. Mater.* **2010**, *22* (20), 2255–2259.

(23) Rubio-Martinez, M.; Imaz, I.; Domingo, N.; Abrishamkar, A.; Mayor, T. S.; Rossi, R.

M.; Carbonell, C.; DeMello, A. J.; Amabilino, D. B.; Maspoch, D.; et al. Freezing the Nonclassical Crystal Growth of a Coordination Polymer Using Controlled Dynamic Gradients. *Adv. Mater.* **2016**, *28* (37), 8150–8155.

(24) Abrishamkar, A.; Suárez–García, S.; Sevim, S.; Sorrenti, A.; Pons, R.; Liu, S.-X.; Decurtins, S.; Aromí, G.; Aguilà, D.; Pané, S.; et al. Pathway Selection as a Tool for Crystal Defect Engineering: A Case Study with a Functional Coordination Polymer. *Appl. Mater. Today* **2020**, *20*, 100632.

(25) Calvo Galve, N.; Abrishamkar, A.; Sorrenti, A.; Di Rienzo, L.; Satta, M.; D'Abramo, M.; Coronado, E.; de Mello, A. J.; Mínguez Espallargas, G.; Puigmartí-Luis, J. Exploiting Reaction-Diffusion Conditions to Trigger Pathway Complexity in the Growth of a MOF. *Angew. Chemie - Int. Ed.* **2021**, *60* (29), 15920–15927.

(26) Rodríguez-San-Miguel, D.; Abrishamkar, A.; Navarro, J. A. R.; Rodriguez-Trujillo, R.; Amabilino, D. B.; Mas-Ballesté, R.; Zamora, F.; Puigmartí-Luis, J. Crystalline Fibres of a Covalent Organic Framework through Bottom-up Microfluidic Synthesis. *Chem. Commun.* **2016**, *52* (59), 9212–9215.

(27) Boclair, J. W.; Braterman, P. S.; Jiang, J.; Lou, S.; Yarberry, F. Layered Double Hydroxide Stability. 2. Formation of Cr(III)-Containing Layered Double Hydroxides Directly from Solution. *Chem. Mater.* **1999**, *11* (2), 303–307.

(28) Taviot-Guého, C.; Halma, M.; Charradi, K.; Forano, C.; Mousty, C. Structural and Electrochemical Characterization of Metallo-Porphyrins Intercalated into ZnCr-Layered Double Hydroxides: Some Evidence of Dimer Formation. *New J. Chem.* **2011**, *35* (9), 1898.

(29) del Arco, M.; Rives, V.; Trujillano, R.; Malet, P. Thermal Behaviour of Zn–Cr Layered Double Hydroxides with Hydrotalcite-like Structures Containing Carbonate or Decavanadate. *J. Mater. Chem.* **1996**, *6* (8), 1419–1428.

(30) Baig, N.; Sajid, M. Applications of Layered Double Hydroxides Based Electrochemical Sensors for Determination of Environmental Pollutants: A Review. *Trends Environ. Anal. Chem.* **2017**, *16*, 1–15.

(31) Shao, M.; Zhang, R.; Li, Z.; Wei, M.; Evans, D. G.; Duan, X. Layered Double Hydroxides toward Electrochemical Energy Storage and Conversion: Design, Synthesis and Applications. *Chem. Commun.* **2015**, *51* (88), 15880–15893.

(32) Zhao, J.; Chen, J.; Xu, S.; Shao, M.; Zhang, Q.; Wei, F.; Ma, J.; Wei, M.; Evans, D. G.; Duan, X. Hierarchical NiMn Layered Double Hydroxide/Carbon Nanotubes Architecture with Superb Energy Density for Flexible Supercapacitors. *Adv. Funct. Mater.* **2014**, *24* (20), 2938–2946.

(33) Latorre-Sanchez, M.; Atienzar, P.; Abellán, G.; Puche, M.; Fornés, V.; Ribera, A.; García, H. The Synthesis of a Hybrid Graphene–Nickel/Manganese Mixed Oxide and Its Performance in Lithium-Ion Batteries. *Carbon N. Y.* **2012**, *50* (2), 518–525.

(34) Hunt, D.; Oestreicher, V.; Mizrahi, M.; Requejo, F. G.; Jobbágy, M. Unveiling the Occurrence of Co(III) in NiCo Layered Electroactive Hydroxides: The Role of Distorted Environments. *Chem. – A Eur. J.* **2020**, *26* (71), 17081–17090.

(35) Arencibia, N.; Oestreicher, V.; Viva, F. A.; Jobbágy, M. Nanotextured Alpha Ni(II)-Co(II) Hydroxides as Supercapacitive Active Phases. *RSC Adv.* **2017**, *7* (10), 5595–5600.

Electronic Supporting Information

# "On-the-fly" synthesis of self-supported LDH hollow structures through controlled microfluidic reaction-diffusion conditions

Michele Mattera,[a] Alessandro Sorrenti,[b] Lidia De Gregorio Perpiñá,[a] Víctor Oestreicher,[c] Semih Sevim,[d] Xiang-Zhong Chen,[e] Salvador Pané,[d] Gonzalo Abellán*[c] and Josep Puigmartí-Luis*[a,f]

a Departament de Ciència dels Materials i Química Física, Institut de Química Teòrica i Computacional, University of Barcelona (UB), 08028 Barcelona, Spain

b Departament de Química Inorgànica i Orgànica (Secció de Química Orgànica), University of Barcelona (UB), 08028 Barcelona, Spain

c Institute of Molecular Science, University of Valencia (UVEG), c/ Catedrático José Beltrán 2, 46980 Paterna, Spain

d Institute of Robotics and Intelligent Systems, ETH Zurich, Tannenstrasse 3, Zurich CH 8092, Switzerland

e Institute of Optoelectronics, State Key Laboratory of Photovoltaic Science and Technology, Shanghai Frontiers Science Research Base of Intelligent Optoelectronics and Perception, Fudan University, Shanghai 200433, People's Republic of China.

f Institució Catalana de Recerca i Estudis Avançats (ICREA), Pg. Lluís Companys 23, 08010 Barcelona, Spain

# Table of Contents


**1 MATERIALS AND METHODS S3**

*1.1 Reagents and solvents S3*

*1.2 Powder X-ray diffraction (PXRD) S3*

*1.3 Scanning Electron Microscopy (SEM) S3*

*1.4 Optical Microscopy (OM) S3*

*1.5 Attenuated Total Reflectance – Fourier Transform Infrared Spectroscopy (ATR-FTIR) S3*

*1.6 Raman spectroscopy S3*

*1.7 Electrical characterization methods S3*

*1.8 Microfluidic device design S3*

*1.9 Microfluidic-based preparation of Zn(II)/Cr(III) LDH structures. S4*

*1.10 Microfluidic-based preparation of LDH@CNT composite structures S4*

*1.11 Microfluidic-based preparation of α-Ni(II)/Co(II) LH structures S4*

**2 SUPPLEMENTARY DATA S5**

**3 REFERENCES S11**

# 1 MATERIALS AND METHODS

## 1.1 Reagents and solvents

Chemicals and reagents used in this work include $ZnCl_2$ (≥ 98%), $CrCl_3 \cdot 6\ H_2O$ (≥ 98%), NaOH pellets (≥ 98%), HCl (12 M), $NiCl_2 \cdot 6\ H_2O$ (≥ 98%), $CoCl_2 \cdot 6\ H_2O$ ((≥ 98%), $NH_4OH$ (14 M) and absolute EtOH (≥ 99%) which were supplied by Sigma-Aldrich. Carbon nanotubes matrix TUBALL-BATT-$H_2O$ was supplied by OCSiAl Europe. Polytetrafluoroethylene (PTFE) 1/16" OD, 1 mm ID, microfluidic tubing was obtained by IDEX Health & Science, LLC, USA.

## 1.2 Powder X-ray diffraction (PXRD)

The obtained structures were mechanically ground into powder, prior to the characterization. Powder XRD measurements were run on a PANalytical XPert PRO MPD theta/theta diffractometer of 240 mm of radius, in a configuration of convergent beam with a focalizing mirror and a transmission geometry where the powder was sandwiched between low absorbing films of polyester mylar of 3.6 microns of thickness.

## 1.3 Scanning Electron Microscopy (SEM)

SEM images were acquired on a FESEM JEOL J-7100-F microscope, using as acceleration voltage 10 kV. The samples were deposited on carbon tape, covered aluminium stubs and later sputtered with ~ 5 nm layer of gold or graphite used for EDS measurements.

## 1.4 Optical Microscopy (OM)

Optical Images and videos, were acquired using a Nikon Stereoscope SMZ-800N, coupled with a Basler camera, operated using Pylon Software.

## 1.5 Attenuated Total Reflectance – Fourier Transform Infrared Spectroscopy (ATR-FTIR)

Infrared Spectra were acquired using an attenuated total reflectance (ATR) Thermo Nicolet 6700 FT-IR, equipped with Ge crystal, in the 4000-400 $cm^{-1}$ spectral range.

## 1.6 Raman spectroscopy

Raman spectra were acquired using a Xplora Invert (HORIBA, France) coupled to an inverted Ti-U Microscope (Nikon, Japan). The parameters used for the spectral acquisition were: objective 40x, laser 532 nm, 25% power, slit 1200 nm/lines, exposure time 120s, 4 accumulations, hole 200 µm, and slit 500 µm.

## 1.7 Electrical characterization methods

The sample was mounted onto a custom electrical chip device (JLPCB, Hong Kong), pasted using silver paste ink and then contacted with copper wire. This system is then connected to a Keithley 6517B source that allows the application of a voltage and record the current flowing in the system.

## 1.8 Microfluidic device design

The microfluidic device was designed using a 3D computer-aided design (CAD) software (SOLIDWORKS 2018). Top and bottom parts of the microfluidic device were machined from polytetrafluoroethylene (PTFE). Specifically, the top part includes ports for three liquid inlets as well as concentric holes for press-fitting both the metallic needle (23G, 0.62 ± 0.02 mm OD, 0.37 ± 0.02 mm ID) and the main channel (i.e., PTFE tubing, 1/16" OD, 1 mm ID), whereas the bottom part acts as a holder for the main channel to keep it straight. The ultimate goal of the design was to induce a laminar concentric flow of two reactant solutions inside the cylindrical main channel, i.e., the PTFE tubing (with a length of 10 cm). With this aim, the top part was designed to press-fit a concentric metallic needle to deliver the solution injected through the middle inlet at the

center of the main channel, while surrounded by the sheath produced by the solutions pumped from the two lateral inlets. The solutions were delivered to the device using a low-pressure syringe pump Nemesys 290N (CETONI GmbH, Germany). Overall, the assembled microfluidic device – which is mainly composed of PTFE and provides high chemical resistance even against harsh chemicals, such as NaOH and HCl) – successfully allows for a concentric hydrodynamic flow focusing inside a cylindrical main channel.

### 1.9 Microfluidic-based preparation of Zn(II)/Cr(III) LDH structures.

The LDH structures were prepared from a 2 M NaOH solution and a solution of the metal precursors in a 2:1 molar ratio, respectively 0.4 M $ZnCl_2$ and 0.2 M $CrCl_3 \cdot 6H_2O$ in a 1 mM HCl solution. In a typical configuration, the NaOH solution was flown through Flow 1, side inlets, while the metal precursor solutions were injected through Flow 2, central inlet at suitable flow rates (see Table S1). The resultant LDH structures (or powder) were collected in distilled water, and separated by hand picking from the mixture of hydroxides, then washed with absolute ethanol, and finally dried at 70ºC for 2h. For comparison, the bulk material was prepared by mixing 2 mL of the metal precursor solution with 1 mL of 2 M NaOH solution under magnetic stirring at room temperature for 2 h (we used the same solutions used for the microfluidic experiments). The resulting purple powder was collected by filtration, washed with distilled water and absolute ethanol, and dried at 70ºC for 2 h.

### 1.10 Microfluidic-based preparation of LDH@CNT composite structures

Carbon nanotubes (CNTs) (10g of TUBALL-BATT-$H_2O$) were added to 25 mL of a 2 M NaOH (40 % w/v), while the solution of the metal precursors was prepared as explained in section 1.9. In a typical experiment, the NaOH solution containing the CNTs was flown through Flow 1, side inlet, while the metal precursor solution was injected through Flow 2, central inlet at TFR 2100 µL/min and FRR 3. The obtained hollow structures were then collected in distilled water, separated by hand picking, washed with absolute ethanol and dried a 70ºC for 2 h.

### 1.11 Microfluidic-based preparation of α-Ni(II)/Co(II) LH structures

The LH structures synthesized in this study were prepared from a 2 M NaOH solution and a solution of the metal precursors in a 2:1 molar ratio, respectively 0.4 M $NiCl_2$ and 0.2 M $CoCl_2 \cdot 6H_2O$ dissolved in a 0.2 M $NH_4Cl$ solution. In a typical experiment, the NaOH solution was flown through Flow 1, side inlet, while the metal precursor solution was injected through Flow 2, central inlet, at TFR of 2100 µL/min and FRR 0.3. The resultant structures were collected in distilled water and were separated by hand picking from the mixture of hydroxides, then washed with absolute ethanol, and finally dried at 70ºC for 2h. For comparison, the bulk material was prepared by mixing 2 mL of the Ni/Co solution and 1 mL of the 2M NaOH solution under magnetic stirring at 55ºC for 24 h. The final product (green powder) was collected by filtration, washed with distilled water and absolute ethanol, and dried at 70ºC for 2 h.

## 2 SUPPLEMENTARY DATA

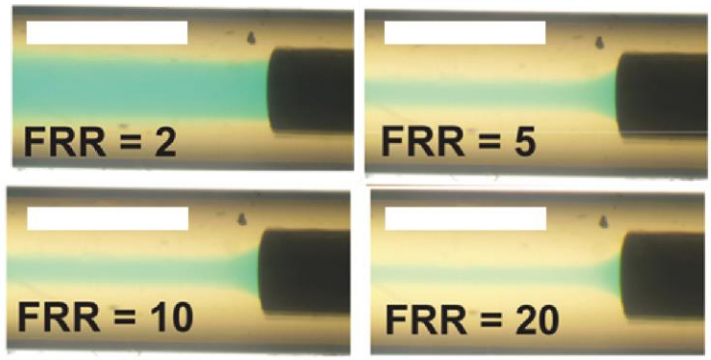


**Figure S1**. Hydrodynamic flow focusing experiments showing the concentric focusing of the central stream (blue food dye) surrounded by a circular shell of sheath flow (DI water) at different flow rate ratio (FRRs), ranging from 2 to 20. The scale bar corresponds to 1.5 mm.

**Table S1.** Influence of FRR and TFR on the morphology of the formed ZnCr LDH structures. The actual flow rate values (in the format 2 x Flow 1 : Flow 2) are reported in italic and expressed in µL/min. Colour code i) non-hollow structures (light green cells); ii) hollow structure (dark green); iii) non-complete hollow structures (light blue); iv) powder LDH (white cells). In the cases ii) and iii) the wall thickness of the hollow structures is expressed in µm and shown in parenthesis.

| | | **FRR** | | | | |
|---|---|---|---|---|---|---|
| | | **10** | **3** | **2** | **1** | **0.3** |
| **TFR (µL/min)** | **1050** | *950:100* | *808:243* | *700:350* | *526:525* | *260:790* |
| | **2100** | *1900:200* (5) | *1614:485* (10) | *1400:700* (8) | *1050:1050* | *520:1580* |
| | **4200** | *3800:480* (4) | *3230:970* (5) | *2800:1400* (14) | *2100:2100* (38) | *1040:3160* |

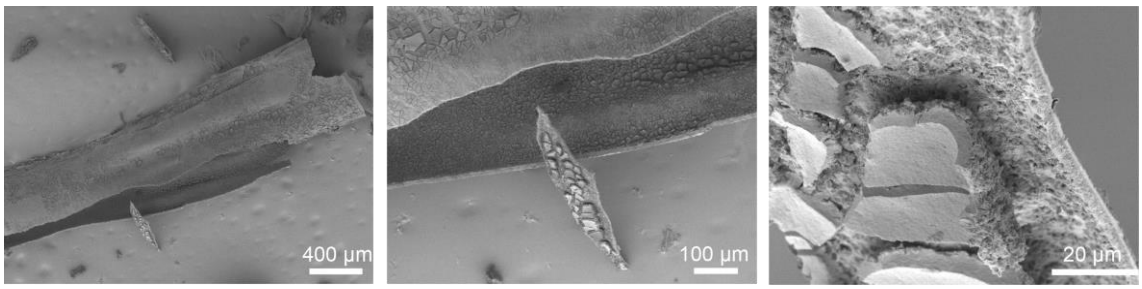


**Figure S2.** SEM images for ZnCr LDH hollow structures obtained at TFR of 2100 µL/min and FRR 3, where it is possible to observe that the external surface of the material is smoother than the internal one.

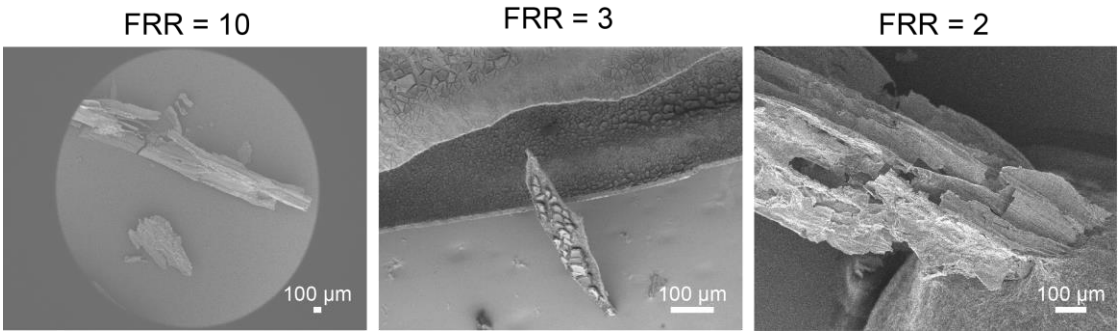


**Figure S3**. SEM images for hollow ZnCr LDH structures obtained at TFR of 2100 µL/min and different FRRs.

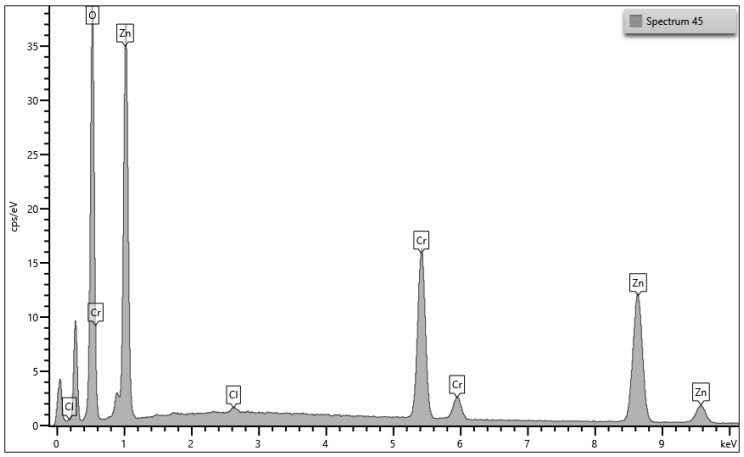


**Figure S4**. EDS spectrum of ZnCr LDH hollow structures prepared by microfluidic synthesis.

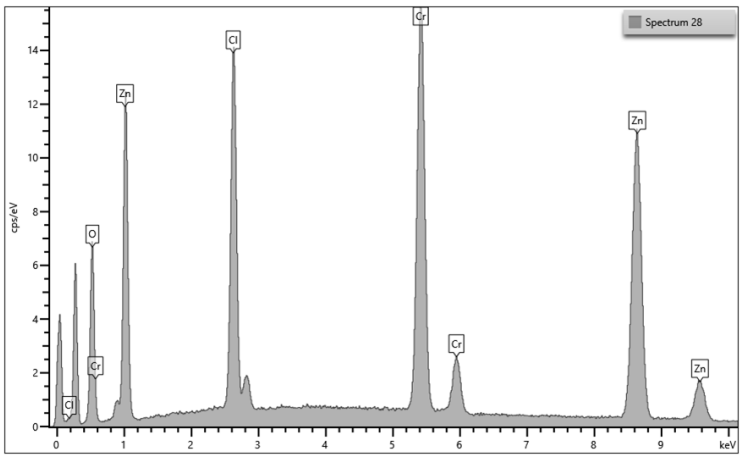


**Figure S5**. EDS spectrum of ZnCr LDH powder material prepared by bulk synthesis.

**Table S2**. Elemental molar percentage calculated from EDS

| Elemental Molar Percentage | O | Cl | Cr | Zn |
|---|---|---|---|---|
| Zn(II)/Cr(III) LDH hollow structures (microfluidic synthesis) | 1.916 | 0.007 | 0.366 | 0.765 |
| Zn(II)/Cr(III) LDH powder (bulk synthesis) | 0.609 | 0.267 | 0.460 | 0.870 |

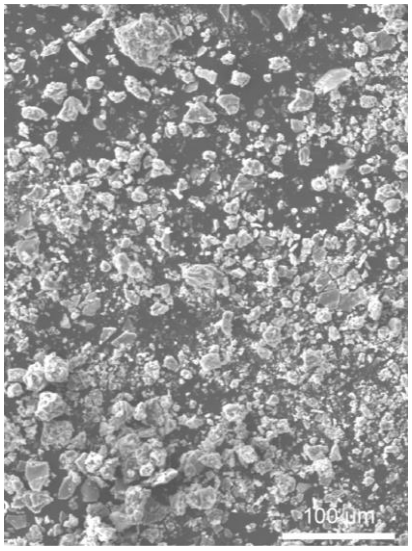


**Figure S6**. SEM image of the ZnCr LDH powder prepared by conventional bulk synthesis.

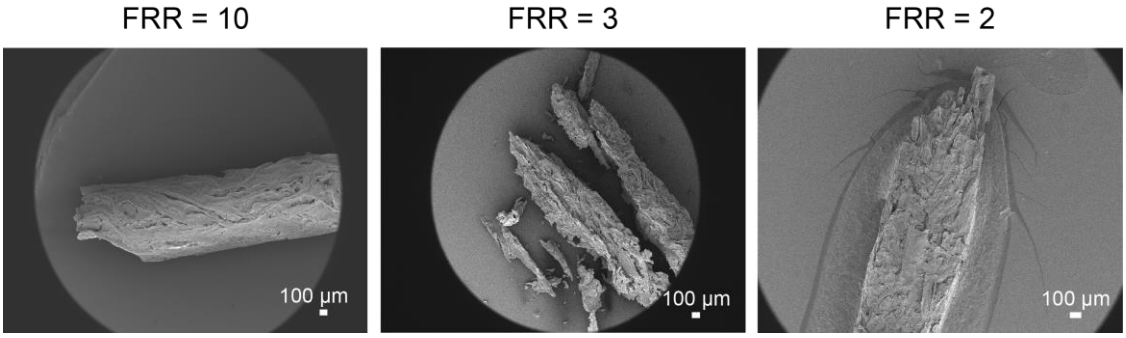


**Figure S7**. SEM images of the non-hollow ZnCr LDH structures obtained by microfluidic synthesis using a TFR of 1050 µL/min and different FRRs.

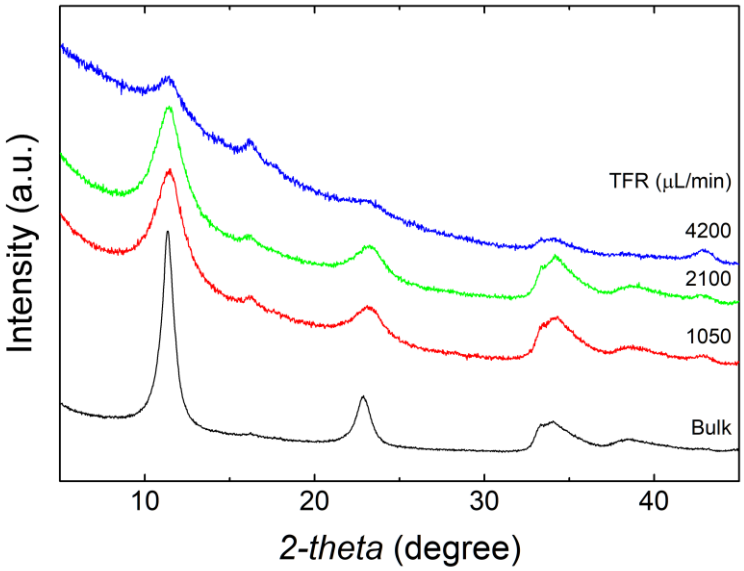


**Figure S8**. PXRD patterns of the ZnCr LDH structures prepared by microfluidic synthesis using increasing TFRs, namely 1050 (red), 2100 (green), and 4200 µL/min (blue) (at FRR 3), compared with the diffraction pattern of the bulk prepared LDH sample (black). Note that the same diffraction pattern is obtained independently of the FRR (i.e., for hollow and non-hollow structures, as well as for powder samples).

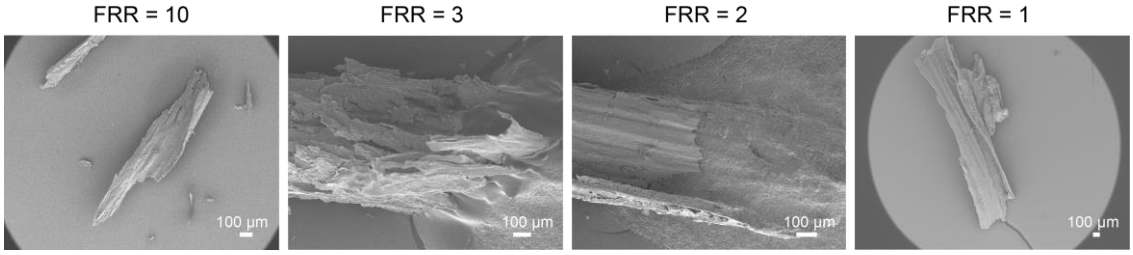


**Figure S9**. SEM images for non-complete hollow ZnCr LDH structures obtained at TFR of 4200 µL/min and different FRRs.

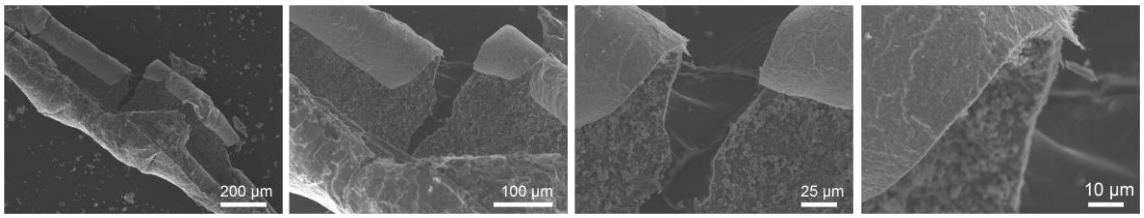


**Figure S10.** SEM images of a ZnCr LDH@CNTs hollow composite structure obtained at TFR 2100 µL/min and FRR 3, where it is possible to observe a network-like layer of CNTs on the external surface.

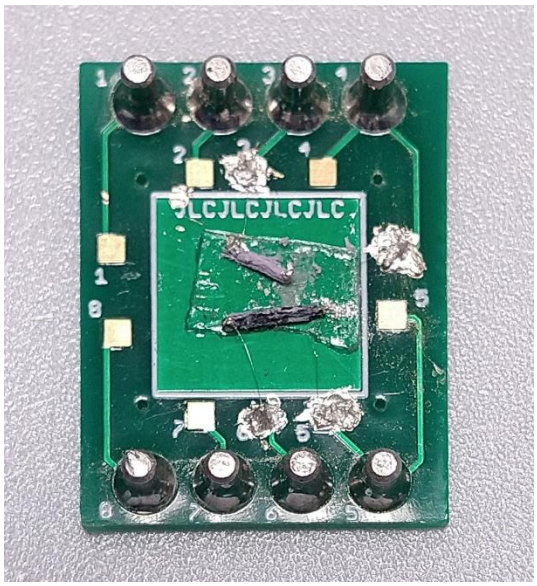

**Figure S11**. Optical micrograph of the electrical chip device, where the hollow structures, respectively ZnCr LDH (top, pink) and ZnCr LDH@CNT composite (bottom, black) are mounted.

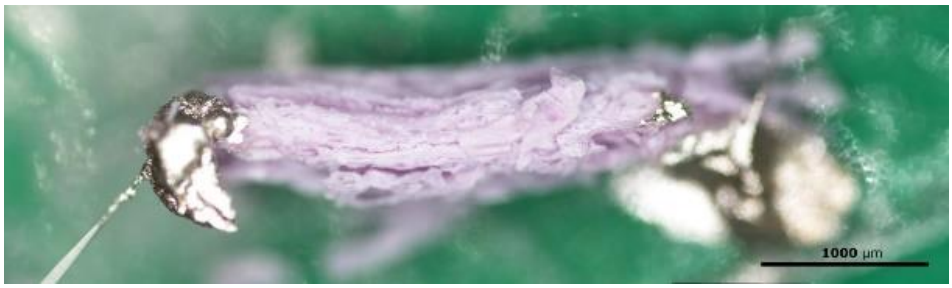


**Figure S12**. Detail of the bare ZnCr LDH hollow structure mounted on the electrical measurement set-up.


**Figure S13**. Detail of the LDH@CNT hollow composite structure mounted on the electrical measurement set-up.

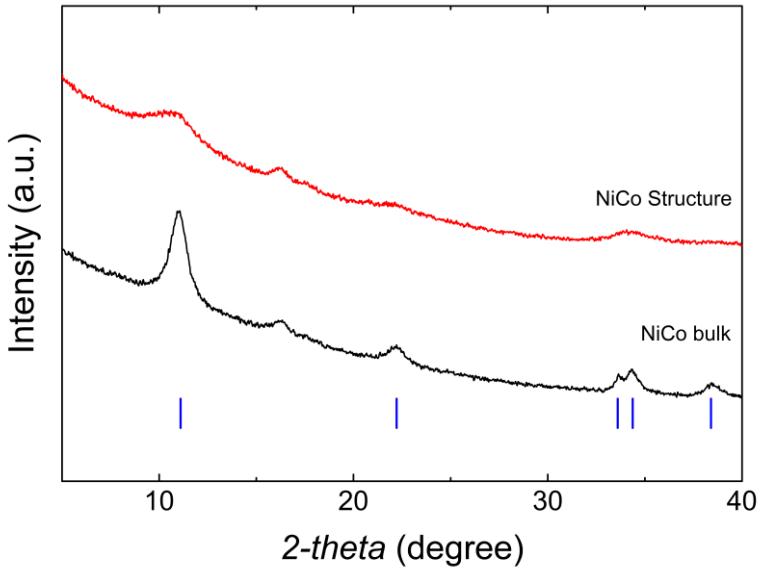


**Figure S14**. PXRD pattern of α-NiCo LH hollow structures prepared at TFR 2100 µL/min and FRR 0.3 (red), compared with the diffraction pattern of the powder sample prepared by bulk synthesis (black). Both exhibiting *simonkolleite*-like (blue) typical reflections.[1]

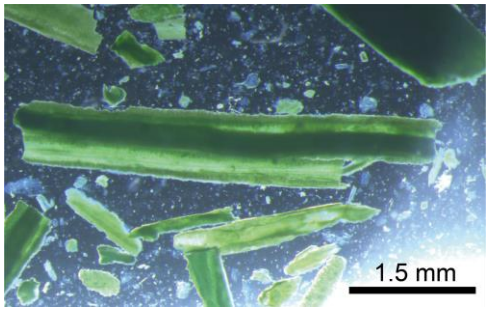


**Figure S15**. Optical micrograph of α-NiCo LH hollow structures obtained at TFR 2100 µL/min and FRR 0.3, showing the intense green colour of the material.

# 3 REFERENCES

(1) Hunt, D.; Oestreicher, V.; Mizrahi, M.; Requejo, F. G.; Jobbágy, M. Unveiling the Occurrence of Co(III) in NiCo Layered Electroactive Hydroxides: The Role of Distorted Environments. *Chem. – A Eur. J.* **2020**, *26* (71), 17081–17090.